doi:10.1016/j.jmb.2008.01.079 J. Mol. Biol. (2008) 377, 647–654

JMB

Available online at www.sciencedirect.com

ScienceDirect

ELSEVIER

COMMUNICATION

Visualisation of a Kinesin-13 Motor on Microtubule End Mimics

Carolyn A. Moores[1]* and Ronald A. Milligan[2]

[1]*School of Crystallography, Birkbeck College, Malet Street, London WC1E 7HX, UK*

[2]*Department of Cell Biology, CB227, The Scripps Research Institute, 10550 North Torrey Pines Road, La Jolla, CA 92037, USA*

Received 23 November 2007; received in revised form 17 January 2008; accepted 23 January 2008
Available online
4 February 2008

Edited by W. Baumeister

An expanding collection of proteins localises to microtubule ends to regulate cytoskeletal dynamics and architecture by unknown molecular mechanisms. Electron microscopy is invaluable for studying microtubule structure, but because microtubule ends are heterogeneous, their structures are difficult to determine. We therefore investigated whether tubulin oligomers induced by the drug dolastatin could mimic microtubule ends. The microtubule end-dependent ATPase of kinesin-13 motors is coupled to microtubule depolymerisation. Significantly, kinesin-13 motor ATPase activity is stimulated by dolastatin–tubulin oligomers, suggesting, first, that these oligomers share properties with microtubule ends and, second, that the physical presence of an end is less important than terminal tubulin flexibility for microtubule end recognition by the kinesin-13 motor. Using electron microscopy, we visualised the kinesin-13 motor–dolastatin–tubulin oligomer interaction in nucleotide states mimicking steps in the ATPase cycle. This enabled us to detect conformational changes that the motor undergoes during depolymerisation. Our data suggest that such tubulin oligomers can be used to examine other microtubule end-binding proteins.

Keywords: depolymerisation; dynamics; electron microscopy; kinesin-13; microtubule; tip-tracking proteins

Microtubules serve as tracks for molecular motors and are essential for many aspects of cellular function. They are dynamic polymers, and the control of growth and shrinkage at their ends is crucial for cytoskeletal regulation. A variety of proteins localise and act at microtubule ends[1,2] so that a key question about microtubule dynamics is by what mechanism(s) do these proteins recognise and regulate microtubule ends? Such a mechanistic questions can be usefully addressed by understanding the structures of the components and the ways in which they interact.

Among the proteins that control microtubule dynamics is the kinesin-13 family of microtubule depolymerising motors. Members of this family are important components of mitotic and meiotic spindles, and they also regulate interphase microtubules.[3] How do kinesin-13 motors depolymerise microtubules at their ends? The fundamental step of microtubule depolymerisation involves an ATP-induced deformation of the terminal tubulin dimer by the kinesin-13 motor domain, pulling the dimer away from its lattice position.[4,5] The minimal kinesin-13 motor core is an inefficient depolymeriser compared with the full-length dimeric kinesin-13,[6–8] but it shares many properties with longer and more efficient kinesin-13 constructs, making it a simple but useful model for the entire family. An important property shared by the motor core and larger constructs is the selective stimulation of the motor ATPase by microtubule ends compared with the microtubule lattice, thereby coupling depolymerisation to ATP turnover.

Because of the size and complexity of microtubules, electron microscopy (EM) is the method of choice for their structural study, and computational analysis of noisy EM images has enabled elucidation of many aspects of microtubule biology.[9] Medium- to high-resolution structure determination by EM relies on averaging data from many nominally identical entities.[10] However, the ends of microtubules are heterogeneous,[11] so that their images

*Corresponding author. E-mail address: c.moores@mail.cryst.bbk.ac.uk.

Abbreviations used: EM, electron microscopy; MSA, multivariate statistical analysis.

cannot be averaged and their structures cannot be calculated using these methods. Tubulin dimers at microtubule ends probably have greater flexibility than dimers constrained within the microtubule lattice, and recognition of this property is postulated to be one mechanism by which microtubule ends are discriminated. Furthermore, the crystal structures of kinesin-13 motor domains suggest that the motor surface is more complementary to the predicted curvature of microtubule ends than to the straight tubulin conformation found in the microtubule lattice.[12,13] Strikingly, dimeric tubulin, which is presumably very flexible, stimulates the kinesin-13 ATPase activity in all constructs examined.[7,8,14] However, for structural purposes, individual tubulin dimers are too small to be visualised by EM.

A number of chemically distinct small molecules are known to perturb the microtubule cytoskeleton by disrupting polymerisation, a property that has made these compounds successful chemotherapeutic agents.[15,16] Several of these molecules stabilise tubulin oligomers, and we reasoned that such oligomers might facilitate our experimental goals of (a) mimicking flexibility at microtubule ends while (b) being large and regular enough to allow analysis of EM images. Dolastatin-10, a peptide derived from the Indian Ocean sea hare *Dolabella auricularia* (Fig. 1a), generates curved tubulin oligomers with

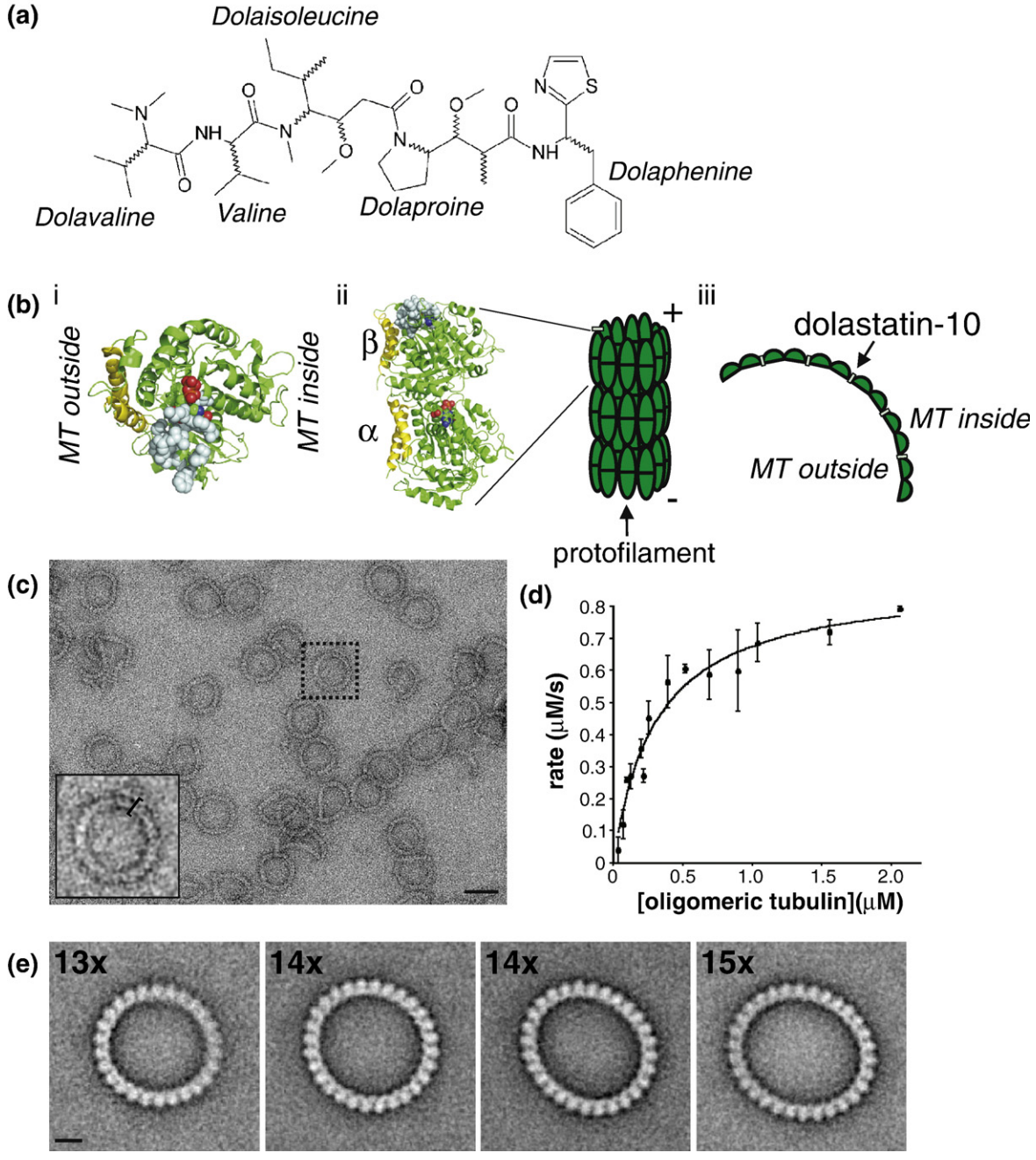

Fig. 1 (*legend on next page*)

an average radial curvature of 220 Å[24,25] that closely matches that adopted by unliganded tubulin.[26,27] A variety of biochemical and modelling experiments[17,19] suggest that the dolastatin binding site is located at the so-called peptide site of the tubulin dimer, on the longitudinal interdimer interface, and close to the nucleotide binding site on β-tubulin (Fig. 1b). This site overlaps, but is not identical, with the vinblastine binding site.[28]

It is essential to understand the motor's interaction with microtubule ends in order to understand the kinesin-13 mechanism. We therefore used the well-studied motor core of kinesin-13 from the malaria parasite (which we call pKinI[5,7,13]) to investigate the ability of dolastatin-induced tubulin oligomers to mimic microtubule ends.

Flexible tubulin oligomers mimic microtubule ends

When tubulin is incubated with dolastatin-10, single protofilaments form curved oligomers such as rings and spirals (Fig. 1c). Crucially for our purposes, dolastatin-10-induced oligomers stimulate the ATPase activity of the kinesin-13 minimal motor domain pKinI to the same extent as tubulin dimers and microtubule ends and in contrast to the inhibition of the pKinI ATPase on binding to the microtubule lattice (Fig. 1d; V_{max} for tubulin–dolastatin oligomers = 0.88 μM/s, *versus* 0.78 μM/s for tubulin heterodimers and 0.63 μM/s for sheared microtubules[7]). This observation is noteworthy because it suggests that it is the relative flexibility of microtubule ends that is the property by which the kinesin-13 motor ATPase is activated, rather than by end-specific surfaces on the terminal tubulins. Tubulin surfaces buried by lateral lattice contacts are more likely to be accessible at microtubule ends and are present in the dolastatin rings as well. Such surfaces might contribute to end recognition mechanisms, but because we are working with a minimal kinesin motor that is well established to interact with the front face of the tubulin dimer, we favour flexibility as the most likely contributing factor to pKinI ATPase activation. Since the plus- and minus-end surfaces of microtubules are structurally very different, this is also consistent with the ability of kinesin-13 motors to depolymerise microtubules at both ends.[4]

Dolastatin-10–tubulin rings imaged by negative-stain EM (Fig. 1c) were processed computationally to allow rings with similar appearances to be averaged together, allowing visualisation of reproducible structural details. The raw images show that the rings are flexible, and this variability of curvature is reflected in the calculated averages (Fig. 1e). The class averages also show that there are three main geometries present in the ring population—13×, 14×, and 15× tubulin dimers, with 14× being the most prevalent, as previously described.[24,25] As expected from the resolution of these images, α-tubulin and

Fig. 1. Dolastatin-10 induces tubulin oligomers that mimic the flexible properties of microtubule ends. (a) Diagram of the pentapeptide dolastatin-10. Previous studies have suggested that the consecutive valine, dolaisoleucine, and dolaproine residues are the most important features for binding to tubulin.[17] This likely accounts for the reduced tubulin affinity of dolastatin-15, a closely related seven-subunit peptide from the same organism that lacks these key residues,[18] and our observation of its failure to induce tubulin oligomers (data not shown). (b-i) View of β-tubulin from the microtubule plus end; residues predicted to bind dolastatin-10 mainly via hydrophobic interaction are shown in space-filling representations in light blue,[17,19] and the bound GDP is shown in space-filling representation in red/green/blue. The tubulin C-terminal α-helices H11 and H12, the principal binding site of kinesin, are shown in yellow. Coordinates from 1SAO.pdb were used.[20] (b-ii) View of the αβ-tubulin heterodimer from the side and relationship of the predicted dolastatin-10 binding site with respect to the microtubule lattice. (b-iii) Schematic of dolastatin-10-induced tubulin oligomers built through protofilament-like longitudinal tubulin contacts and viewed from the side. (c) Electron micrograph of dolastatin-10-induced tubulin oligomers, visualised by negative stain. Bar represents 400 Å. The inset shows the image of an individual ring (boxed) that has been bandpass filtered to reveal more clearly the single band of tubulin density from which the rings are built. Dolastatin-10, dissolved in dimethyl sulfoxide, was incubated with tubulin (purchased from Cytoskeleton, Inc., Denver, CO) at a molar ratio of 2:1 in polymerisation buffer (40 mM Pipes, pH 6.8, 1.5 mM $MgCl_2$, and 12% dimethyl sulfoxide) for 1 h at room temperature. Oligomers were diluted in BrB_{20} [20 mM Pipes, 2 mM $MgCl_2$, 1 mM ethylene glycol bis(β-aminoethyl ether)*N*,*N*′-tetraacetic acid, pH 6.8] prior to use. Tubulin–dolastatin rings (1 μM) were applied to home-made continuous carbon EM grids glow discharged in the presence of amylamine. The rings were negatively stained using 1% uranyl acetate. Images of the dolastatin rings were collected on SO-163 photographic film on a Phillips CM120 electron microscope operating at 100 kV under low-dose conditions and at a nominal magnification of 45,000×. Micrographs were digitised using a Zeiss SCAI microdensitometer with a final pixel size at the sample of 3.1126 Å/pixel (calibrated using Tobacco Mosaic Virus). (d) Stimulation of pKinI ATPase by dolastatin-10-induced tubulin oligomers. V_{max} = 0.88 μM/s; K_m = 0.31 μM; n = 2–4 for each data point; error bars indicate standard deviation. pKinI was prepared as previously described and dialysed against BrB_{20}/1 mM DTT prior to use.[5] The ATPase activity of pKinI (0.25 μM) at 25 °C was measured using an NADH-coupled system as described previously.[7] (e) Representative image averages of dolastatin-10–tubulin rings; the averages contain 93 (13×), 91 (14×), 111 (second average at 14×), and 114 (15×) individual images. Bar represents 100 Å. For image analysis, dolastatin–tubulin rings were selected manually using the MRC program Ximdisp[21]; their defocus was calculated using the MRC program CTFFIND2, and phases were corrected for the contrast transfer function using SPIDER.[22] Individual images were bandpass filtered, normalised, and centred using SPIDER to a rotational average of the previously calculated pKinI-induced tubulin ring.[5] Centred images were then subjected to multivariate statistical analysis (MSA) and classification in IMAGIC.[23] Selected class averages were used iteratively for further rounds of multireference alignment until the outcome of MSA had stabilised (approximately two additional rounds of alignment).

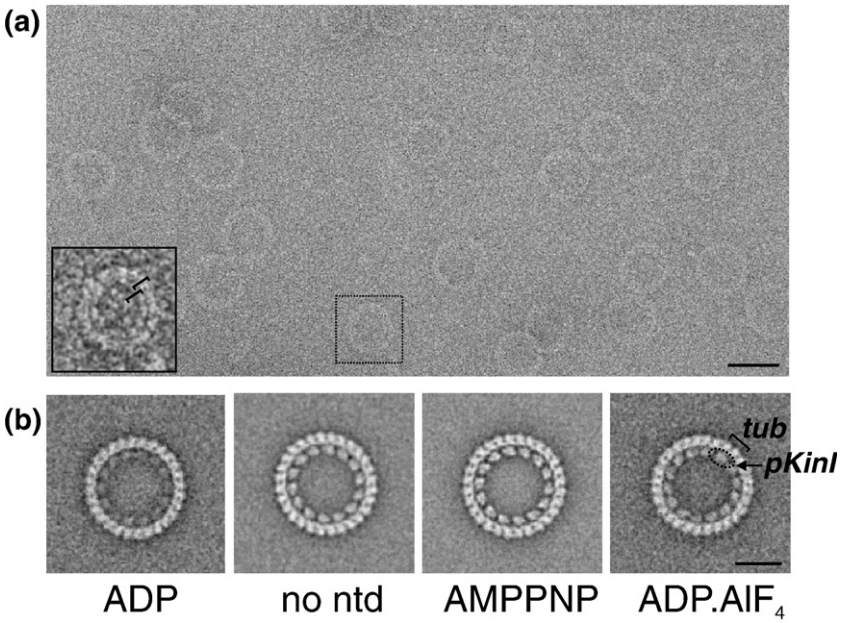

Fig. 2. Nucleotide-dependent interaction of pKinI with dolastatin-10-induced tubulin rings. (a) Electron micrograph of pKinI–AMPPNP bound to dolastatin-10–tubulin rings. Bar represents 400 Å. The inset shows the image of an individual ring (boxed) that has been bandpass filtered to reveal more clearly the double band of density from which the rings are built; the inner layer corresponds to pKinI, which binds to the outer ring of tubulin. The background on this micrograph is high compared with that of Fig. 1c due to the presence of unbound pKinI. Tubulin–dolastatin rings (1 μM) were incubated with 5 μM pKinI and 1 mM nucleotide or nucleotide analogue (ADP, AMPPNP, ADP.AlF_4, or in the absence of nucleotide) for 5 min at room temperature, and these mixtures were prepared and imaged by EM as described in the legend to Fig. 1. (b) Representative image averages of pKinI–dolastatin-10–tubulin rings with 14× geometry in different nucleotide states; the averages contain 102 (ADP), 187 (no nucleotide), 193 (AMPPNP), and 84 (ADP.AlF_4) individual images and were calculated as described in the legend to Fig. 1. The ring averages show a marked handedness, demonstrated by the skew of the tubulin in the outside ring and the direction in which the pKinI density faces on the inner ring; this handedness is clockwise for the rings in the absence of nucleotide and in the presence of AMPPNP and counterclockwise for ADP and ADP.AlF_4, and is a reflection of the way in which the rings fall on the grid and of the fact that each nucleotide data set was processed independently. Bar represents 200 Å.

β-tubulin cannot be discriminated; neither do the structural details around the rings show repetitive variation that would allow intra- and interdimer interfaces to be identified. This suggests that intra- and interdimer curvatures are not correlated (or that differences are undetectable) in these images. This is in contrast to the tubulin oligomers induced by the peptide cryptophycin,[29] demonstrating the variety of tubulin oligomeric forms induced by peptides binding at very similar sites on β-tubulin. The similarity of dolastatin–tubulin and unliganded tubulin oligomer curvatures, as well as their ability to

Fig. 3. Conformational changes in pKinI during its ATPase cycle. (a) Averages of the pKinI–tubulin dimer repeat for each nucleotide state. These were calculated as follows: following calculation of the pKinI–dolastatin–tubulin ring class averages, the best classes were evaluated for homogeneity by MSA and by visual inspection of their constituent members prior to further processing. At no point was 14-fold rotational symmetry imposed. From the best 14× averages for each nucleotide state, individual pKinI–tubulin dimer complexes were picked manually and were aligned. These steps are illustrated in Supplementary Fig. 1c. For the ADP, no nucleotide, AMPPNP, and ADP.AlF_4 states, 4, 5, 7, and 7 class averages, respectively, were used, generating 40, 70, 98, and 98 individual pKinI–tubulin dimer units, respectively. ADP rings were incompletely decorated, so only segments with an obvious motor density were selected. An average and variance map for each nucleotide state was calculated, and the statistically significant differences between states, representing nucleotide-dependent conformational changes, were evaluated pixel by pixel using Student's *t*-tests.[30] The statistically significant differences between half data sets of the same nucleotide state were examined, and in all cases were found to be minimal in comparison with differences between nucleotide states, confirming the validity of these observations. Differences between the nucleotide states calculated using the *t*-tests analysis were confirmed using MSA in IMAGIC. (b) Schematic of the kinesin-13 ATPase cycle at the microtubule end; the steps are numbered according to the corresponding panels in (c). (c) Evaluation of the statistically significant differences between consecutive nucleotide states in the ATPase cycle (indicated beneath) representing conformational changes in the motor. The right-hand column shows the output of Student's *t*-tests, contoured at a probability of <0.005. The positions of these peaks of statistically significant difference are indicated on the relevant image averages with red circles. (d) Model of the pKinI–tubulin interaction obtained by docking pKinI (1RY6.pdb)[13] onto GDP–tubulin (1SA0.pdb).[20] This docking was performed using KIF1A–tubulin coordinates (2HXH.pdb)[31] as a template in PyMOL [http://www.pymol.org] and is consistent with other kinesin–tubulin structures.[7,12,32] The pKinI–GDP–tubulin atomic model is presented such that it matches the EM projection maps as closely as possible. pKinI is shown in blue, and the GDP–tubulin dimer is shown in green; a space-filling model of ADP indicates the kinesin nucleotide binding site, although no nucleotide was found in the pKinI crystal structure. The pKinI relay helix, α4, is coloured yellow and sits at the tubulin intradimer interface; this region of pKinI appears to be invariant during ATP binding and hydrolysis steps. Other portions of pKinI likely to be involved in conformational changes during the motor's ATPase cycle are depicted in red and include loop 2 (L2), which contains kinesin-13 depolymerisation-specific residues; helix 6 (α6); loop 12/helix 5 (L12/α5); and loop 8 (L8).

stimulate pKinI ATPase, encouraged us to examine the interaction between pKinI and dolastatin rings more closely. Using EM and image analysis of the pKinI–ring complexes, we dissected the nucleotide-dependent interaction of the motor with these microtubule end mimics.

Nucleotide-dependent interaction of pKinI with rings visualised by EM

Raw images of pKinI–dolastatin-10–tubulin rings show the presence of additional protein density on the inside of the tubulin rings (corresponding to the

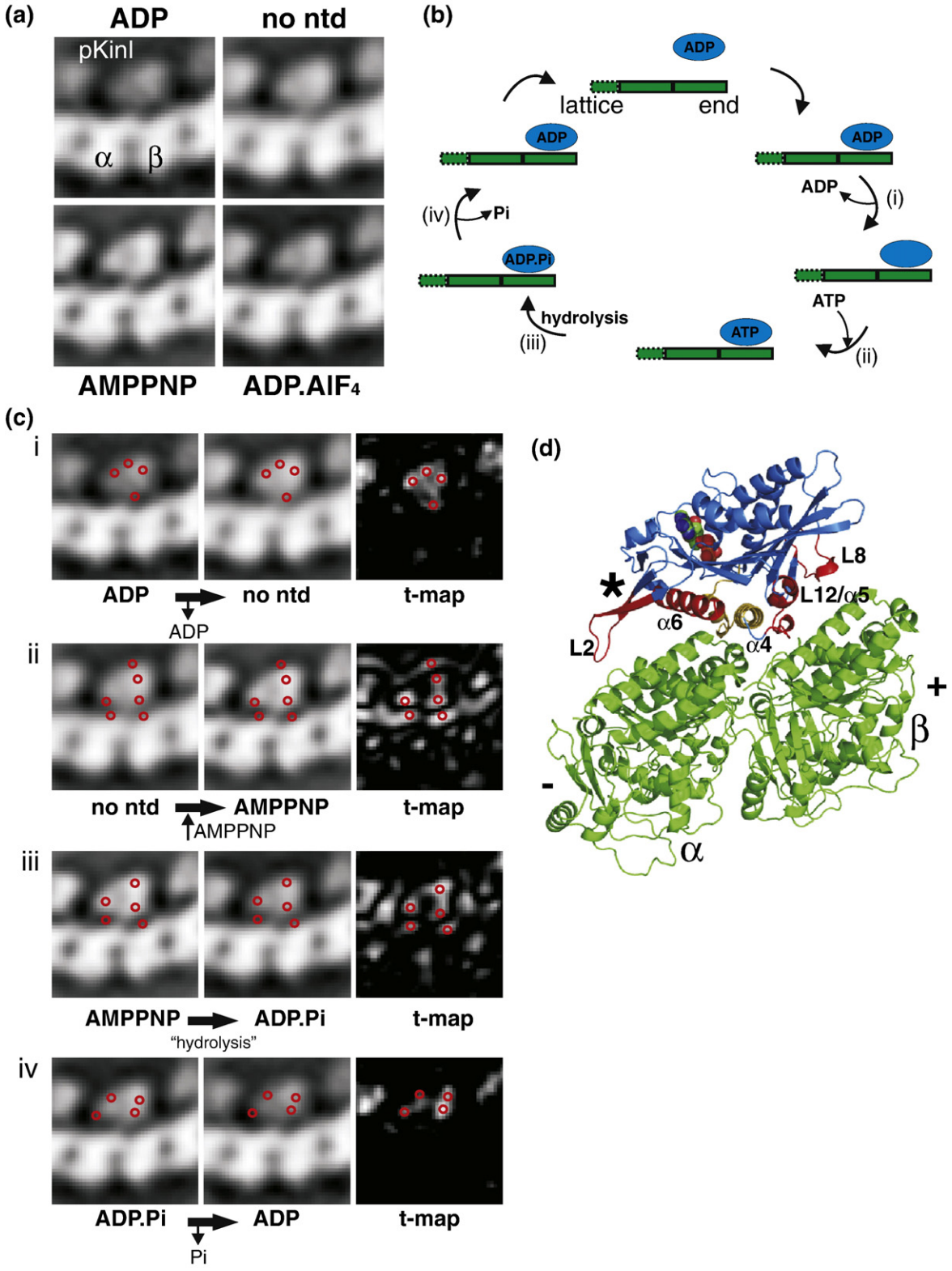

Fig. 3 (*legend on previous page*)

microtubule external surface; Figs. 1b and 2a). Dolastatin–tubulin rings also appear less flexible in the presence of pKinI, suggesting that at least part of the ring flexibility is constrained by motor binding (compare Fig. 1c with Fig. 2a). Despite this, the pKinI-bound dolastatin-10–tubulin rings were not perfectly circular, suggesting the presence of some residual flexibility at the interdimer contacts where dolastatin-10 is presumed to bind. We examined pKinI–ring complexes in the presence of ADP, no nucleotide, AMPPNP (a non-hydrolysable ATP analogue), and ADP.AlF_4 (a transition-state analogue, mimicking ADP.P_i), thereby capturing different stages of the pKinI ATPase cycle. Representative averages for each nucleotide state are shown in Fig. 2b. In each, density corresponding to the pKinI motor associates with two tubulin densities, as is typical for kinesin motors. We observed good pKinI binding in all nucleotide states apart from ADP, where the motor density is more poorly defined. In all cases, 13×, 14×, and 15× geometries were observed (Supplementary Fig. 1a), but the 14× geometry provided the majority of the data for each nucleotide state (an average of 63% of the data compared with averages of 14% and 23% for the 13× and 15× geometries, respectively).

Nucleotide-dependent conformational changes by pKinI bound to tubulin rings

To further probe the nucleotide-dependent conformational state of pKinI on the tubulin rings, we wanted to combine data of the motor–tubulin complex from the individual 14× averages and around each ring. Since the rings are built from nominally identical pKinI–tubulin dimer repeats, further averaging of these individual building blocks should enable additional structural details to be extracted. However, simple rotational averaging results in degradation of the average because the rings are not perfectly circular and such rotational averaging was never imposed (Supplementary Fig. 1). Instead, we selected the pKinI–tubulin dimer units from the best 14× class averages for each nucleotide state (treating each motor–tubulin dimer repeat in the ring averages as a single particle) and aligned and averaged these together to create a pKinI–tubulin dimer image for each nucleotide state. These averages demonstrate that there are only very small changes in the tubulin in the different nucleotide states but that pKinI passes through a series of distinct conformational states during its ATPase cycle (Fig. 3a and b). To understand these pKinI states in more detail, we used Student's *t*-test to calculate the statistically significant differences between nucleotide states of pKinI (Fig. 3c).[30] As data shown in these averages are moderate-resolution two-dimensional projections of the three-dimensional structure of the motor–tubulin complex, we have interpreted the nucleotide-dependent differences we observed conservatively. To facilitate this interpretation and provide an overview of the changes occurring in the motor domain during its ATPase cycle at microtubule ends, we generated an atomic model of the pKinI–tubulin interaction based on available structural information (Fig. 3d). The pKinI interaction with tubulin is centred on helix-α4, the nucleotide-sensing switch II relay helix (shown in yellow),[33] which sits above the tubulin intradimer interface. Towards the plus end, residues in loop 12/helix-α5 and loop 8 of the motor lie close to the β-tubulin surface, while at the minus end, helix-α6 and loop 2, containing residues essential for depolymerisation, are close to α-tubulin (shown in red).[12,13]

On binding of pKinI to tubulin, ADP is released from the motor, and, according to our data, this is coupled to conformational changes in pKinI that are spread across most of the motor domain. The overall shape of the *t*-map in Fig. 3c-i resembles that of the motor domain, reflecting the incomplete occupancy of pKinI–ADP binding and suggesting that, in the absence of nucleotide, pKinI sits more firmly on the terminal tubulin following ADP dissociation. This is in contrast to the localised conformational change we identified in pKinI when it released ADP on interaction with the microtubule lattice.[7] The more widespread changes we observed when pKinI bound to dolastatin–tubulin rings likely reflect engagement of the entire kinesin-13 motor domain with its tubulin substrate in preparation for ATP binding and hydrolysis, neither of which can occur on the non-flexible microtubule wall.[7]

We previously described induction of curled protofilaments by pKinI–AMPPNP from the ends of stabilised microtubules that likely represent a key step in microtubule depolymerisation.[5] In our current experiments, we observed pKinI on curved tubulin that is longitudinally constrained by the ring, so we did not expect to see additional curving in the tubulin when AMPPNP (mimicking ATP) bound to pKinI. Nevertheless, on AMPPNP binding, pKinI apparently undergoes concerted conformational changes, with alterations at the pKinI–tubulin interface dominating the *t*-map (Fig. 3c-ii). One cluster of statistically significant differences is located towards the motor's plus end in regions that correspond to important elements of kinesin's energy transduction system, including helix-α5/loop 12 and loop 8. Loop 12 is conserved in all kinesins and is thought to be important in kinesin–microtubule interactions,[34] while the nearby loop 8 has been proposed to act as a sensor for regulation of ATP hydrolysis in depolymerising kinesins.[12] At the motor's minus end, there are also conformational changes in pKinI close to the surface of tubulin—these probably involve α6 and the kinesin-13-specific loop 2 region. It seems likely that the extended conformation of loop 2 seen in the crystal structure will alter when pKinI is bound to its tubulin substrate. These clusters of conformational changes occur at either end of the motor on either side of an apparently static anchor point that is likely to be formed, at least in part, by helix-α4. It is interesting to note that this mirrors the behaviour of the functionally very different kinesin KIF1A, in which the kinesin motor domain was observed to rearrange

itself around its fixed relay helix during its ATPase cycle.[31]

Similar regions of the motor appear to alter their conformations when ATP is hydrolysed by pKinI (Fig. 3c-iii). However, while major changes near the tubulin surface were observed on ATP binding, changes in the body of the motor itself are more significant on ATP hydrolysis. It has previously been postulated that the hydrolysis step of the kinesin-13 ATPase cycle is important for release of the terminal tubulin from the microtubule end.[4] In the context of the dolastatin rings, such release is probably prevented because the tubulin to which pKinI is attached is constrained at both ends. Our data are consistent with this idea and are further supported by the widespread differences in pKinI when comparing the ADP.P_i and ADP states, suggesting that release of pKinI from its tubulin substrate is coupled to phosphate release (Fig. 3c-iv).

Our data have revealed the dynamic response of the kinesin-13 motor domain that allows coupling of ATP turnover to depolymerisation at microtubule ends. What might we predict for larger kinesin-13 constructs including the native dimer? The kinesin-13 neck sequence, not present in our pKinI construct, is essential for efficient motor activity, although the precise mechanism by which it acts is unknown.[6] In a recently solved crystal structure (2gry.pdb†), the proximal part of the kinesin-13 neck helix (the only part of the neck that is visible) lies directly above loop 2 (its position is indicated by the asterisk in Fig. 3d). In light of our data, one possible mechanism by which the neck sequence could be involved in motor efficiency is by direct coupling of the neck to conformational changes in the motor core during the ATP binding and hydrolysis steps, perhaps enabling amplification of these conformational changes and transmission to adjacent protofilaments of the microtubule.[35] The contributions of the rest of the kinesin-13 protein to and the significance of dimerisation for the depolymerisation mechanism are less clear. Further experiments will aim to probe these questions and to establish the role of the actual microtubule end in depolymerisation efficiency.

Cell biology studies have told us a great deal about the location and colocalisation of a large number of proteins at the dynamic ends of microtubules,[2] but we know very little about the detailed molecular mechanisms by which microtubule ends are identified. Our ability to observe the activity and conformational changes of an end-specific motor using dolastatin-induced rings has provided insight into important properties of microtubule ends that distinguish them from the bulk microtubule cytoskeleton. These rings could be extremely useful in discriminating between different binding mechanisms of the many proteins that are active at microtubule ends and to visualise the variety of protein–protein interactions that are found there.[36,37]

† http://www.rcsb.org/pdb

Acknowledgements

Part of the work presented here was conducted at the National Resource for Automated Molecular Microscopy, which is supported by the National Institutes of Health through the National Center for Research Resources' P41 Program (RR17573). We gratefully thank Professor G.R. Pettit (Arizona State University, Tempe, AZ) for providing dolastatin-10 and Cytokinetics, Inc. (South San Francisco, CA) for providing recombinant pKinI protein. We also thank Yulia Ovechkina and Linda Wordeman (University of Washington, Seattle, WA) for suggesting we pursue this experimental approach. C.A.M. is a BBSRC David Phillips Fellow, and R.A.M. is supported by grant GM52468 from the National Institutes of Health.

Supplementary Data

Supplementary data associated with this article can be found, in the online version, at doi:10.1016/j.jmb.2008.01.079

References

1. Howard, J. & Hyman, A. (2003). Dynamics and mechanics of the microtubule plus end. *Nature*, **422**, 753–758.
2. Morrison, E. E. (2007). Action and interactions at microtubule ends. *Cell. Mol. Life Sci.* **64**, 307–317.
3. Moores, C. A. & Milligan, R. A. (2006). Lucky 13—microtubule depolymerisation by kinesin-13 motors. *J. Cell Sci.* **119**, 3905–3913.
4. Desai, A., Verma, S., Mitchison, T. J. & Walczak, C. E. (1999). Kin I kinesins are microtubule-stabilizing enzymes. *Cell*, **96**, 69–78.
5. Moores, C. A., Yu, M., Guo, J., Beraud, C., Sakowicz, R. & Milligan, R. A. (2002). A mechanism for microtubule depolymerisation by KinI kinesins. *Mol. Cell*, **9**, 903–909.
6. Ovechkina, Y., Wagenbach, M. & Wordeman, L. (2002). K-loop insertion restores microtubule depolymerizing activity of a "neckless" MCAK mutant. *J. Cell Biol.* **159**, 557–562.
7. Moores, C. A., Hekmat-Nejad, M., Sakowicz, R. & Milligan, R. A. (2003). Regulation of KinI kinesin ATPase activity by binding to the microtubule lattice. *J. Cell Biol.* **163**, 963–971.
8. Ems-McClung, S. C., Hertzer, K. M., Zhang, X., Miller, M. W. & Walczak, C. E. (2007). The interplay of the N- and C-terminal domains of MCAK control microtubule depolymerization activity and spindle assembly. *Mol. Biol. Cell*, **18**, 282–294.
9. Nogales, E. (2001). Structural insight into microtubule function. *Annu. Rev. Biophys. Biomol. Struct.* **30**, 397–420.
10. Hoenger, A. & Nicastro, D. (2007). Electron microscopy of microtubule-based cytoskeletal machinery. *Methods Cell Biol.* **79**, 437–462.
11. Mandelkow, E. M., Mandelkow, E. & Milligan, R. A. (1991). Microtubule dynamics and microtubule caps: a time-resolved cryo-electron microscopy study. *J. Cell Biol.* **114**, 977–991.
12. Ogawa, T., Nitta, R., Okada, Y. & Hirokawa, N. (2004).

A common mechanism for microtubule destabilisers—M type kinesins stabilize curling of the protofilament using the class-specific neck and loops. *Cell*, **116**, 591–602.
13. Shipley, K., Hekmat-Nejad, M., Turner, J., Moores, C., Anderson, R., Milligan, R. *et al.* (2004). Structure of a kinesin microtubule depolymerisation machine. *EMBO J.* **23**, 1422–1432.
14. Hunter, A. W., Caplow, M., Coy, D. L., Hancock, W. O., Diez, S., Wordeman, L. & Howard, J. (2003). The kinesin-related protein MCAK is a microtubule depolymerase that forms an ATP-hydrolysing complex at microtubule ends. *Mol. Cell*, **11**, 445–457.
15. Prinz, H. (2002). Recent advances in the field of tubulin polymerisation inhibitors. *Expert Rev. Anticancer Ther.* **2**, 695–708.
16. Rawat, D. S., Joshi, M. C., Joshi, P. & Atheaya, H. (2006). Marine peptides and related compounds in clinical trial. *Anticancer Agents Med. Chem.* **6**, 33–40.
17. Mitra, A. & Sept, D. (2004). Localisation of the antimitotic peptide and depsipeptide binding site on β-tubulin. *Biochemistry*, **43**, 13955–13962.
18. Bai, R., Friedman, S. J., Pettit, G. R. & Hamel, E. (1992). Dolastatin 15, a potent antimitotic depsipeptide derived from *Dolabella auricularia*. Interaction with tubulin and effects of cellular microtubules. *Biochem. Pharmacol.* **43**, 2637–2645.
19. Bai, R., Covell, D. G., Taylor, G. F., Kepler, J. A., Copeland, T. D., Nguyen, N. Y. *et al.* (2004). Direct photoaffinity labelling by dolastatin-10 of the amino-terminal peptide of β-tubulin containing cysteine 12. *J. Biol. Chem.* **279**, 30731–30740.
20. Ravelli, R. B., Gigant, B., Curmi, P. A., Jourdain, I., Lachkar, S., Sobel, A. & Knossow, M. (2004). Insight into tubulin regulation from a complex with colchicine and a stathmin-like domain. *Nature*, **428**, 198–202.
21. Crowther, R. A., Henderson, R. & Smith, J. M. (1996). MRC image processing programs. *J. Struct. Biol.* **116**, 9–16.
22. Frank, J., Radermacher, M., Penczek, P., Zhu, J., Li, Y., Ladjadj, M. & Leith, A. (1996). SPIDER and WEB: processing and visualisation of images in 3D electron microscopy and related fields. *J. Struct. Biol.* **116**, 190–199.
23. van Heel, M., Harauz, G., Orlova, E. V., Schmidt, R. & Schatz, M. (1996). A new generation of the IMAGIC image processing system. *J. Struct. Biol.* **116**, 17–24.
24. Bai, R., Durso, N. A., Sackett, D. L. & Hamel, E. (1999). Interactions of the sponge-derived antimitotic tripeptide hemiasterlin with tubulin: comparison with dolastatin 10 and cryptophycin 1. *Biochemistry*, **38**, 14302–14310.
25. Boukari, H., Sackett, D. L., Schuck, P. & Nossal, R. J. (2007). Single-walled tubulin ring polymers. *Biopolymers*, **86**, 424–436.
26. Müller-Reichert, T., Chrétien, D., Severin, F. & Hyman, A. A. (1998). Structural changes at microtubule ends accompanying GTP hydrolysis: information from a slowly hydrolysable analogue of GTP, guanylyl (α,β) methylenediphosphonate. *Proc. Natl Acad. Sci. USA*, **95**, 3661–3666.
27. Nicholson, W. V., Lee, M., Downing, K. H. & Nogales, E. (1999). Cryo-electron microscopy of GDP–tubulin rings. *Cell Biochem. Biophys.* **31**, 175–183.
28. Gigant, B., Wang, C., Ravelli, R. B. G., Roussi, F., Steimetz, M. O., Curmi, P. A. *et al.* (2005). Structural basis for the regulation of tubulin by vinblastine. *Nature*, **435**, 519–522.
29. Watts, N. R., Cheng, N., West, W., Steven, A. C. & Sackett, D. L. (2002). The cryptophycin–tubulin ring structure indicates two points of curvature in the tubulin dimer. *Biochemistry*, **41**, 12662–12669.
30. Milligan, R. A. & Flicker, P. F. (1987). Structural relationships of actin, myosin, and tropomyosin revealed by cryo-electron microscopy. *J. Cell Biol.* **105**, 29–39.
31. Kikkawa, N. & Hirokawa, N. (2006). High-resolution cryo-EM maps show the nucleotide binding pocket of KIF1A in open and closed conformations. *EMBO J.* **25**, 4187–4194.
32. Sindelar, C. & Downing, K. H. (2007). The beginning of kinesin's force-generating cycle visualized at 9-Å resolution. *J. Cell Biol.* **177**, 377–385.
33. Vale, R. D. & Milligan, R. A. (2000). The way things move: looking under the hood of molecular motor proteins. *Science*, **288**, 88–95.
34. Woehlke, G., Ruby, A. K., Hart, C. L., Ly, B., Hom-Booher, N. & Vale, R. D. (1997). Microtubule interaction site of the kinesin motor. *Cell*, **90**, 207–216.
35. Moores, C. A., Cooper, J., Wagenbach, M., Ovechkina, Y., Wordeman, L. & Milligan, R. A. (2006). The role of the kinesin-13 neck in microtubule depolymerization. *Cell Cycle*, **5**, 1812–1815.
36. Honnappa, S., Okhrimenko, O., Jaussi, R., Jawhari, H., Jelesarov, I., Winkler, F. K. & Steinmetz, M. O. (2006). Key interaction modes of dynamic +TIP networks. *Mol. Cell*, **23**, 663–671.
37. Slep, K. C. & Vale, R. D. (2007). Structural basis of microtubule plus end tracking by XMAP215, CLIP-170, and EB1. *Mol. Cell*, **27**, 976–991.